Heliyon 9 (2023) e20642

Contents lists available at ScienceDirect

Heliyon

journal homepage: www.cell.com/heliyon

Accuracy of attenuation coefficient measurement (ACM) for real-time ultrasound hepatic steatometry: Comparison of simulator/phantom data with magnetic resonance imaging proton density fat fraction (MRI-PDFF)

Nazarii Kobyliak [a,b,*], Oleh Dynnyk [c], Maryana Savytska [d], Oleksandr Solodovnyk [e], Oleksandr Zakomornyi [e], Oleksii Omelchenko [e], Anton Kushnir [f], Roman Titorenko [f]

[a] *Endocrinology Department, Bogomolets National Medical University, 01601, Kyiv, Ukraine*
[b] *Medical Laboratory CSD, 03022, Kyiv, Ukraine*
[c] *Medical Center "Institute of elastography" LLC, Kyiv, Ukraine*
[d] *Normal Physiology Department, Danylo Halytsky Lviv National Medical University, Lviv, Ukraine*
[e] *Medical Center "Varta" of "Vision Partner" LLC, Kyiv, Ukraine*
[f] *"Mediscan Group" LLC, Kyiv, Ukraine*

ARTICLE INFO

Keywords:
Attenuation coefficient
Hand held US device
MRI-PDFF
POCUS
Liver steatosis
Ultrasound

ABSTRACT

Objectives: To evaluate the accuracy and reproducibility of real time ultrasound (US) steatometry with the Attenuation Coefficient (AC) measurement in comparison with magnetic resonance imaging with proton density software module (MRI-PDFF).
Methods: This study was conducted between January 2021 and October 2021. The comparison of instrumental methods for assessing and grading hepatic steatosis using a multimodal phantom simulator of different fat and water ratios was performed. The study involved 3 radiological centers. The steatophantom was simultaneously investigated using three methods: magnetic resonance imaging with proton density software module (MRI-PDFF) and 128-slice multidetector computed tomography, and then by 2 different US scanner for steatosis assessment via Measurement Attenuation Imaging (ATI) ant Attenuation Coefficient Measurement (ACM).
Results: Modeling of hepatic steatosis using a series of phantom simulators allows evidence-based medicine to determine the diagnostic accuracy of the latest US techniques for steatosis. The ACM and ATI of both US systems on phantoms correlated well with each other and with MRI-PDFF and, thus, can provide good diagnostic value in the assessment of hepatic steatosis. MDCT was less sensitive to mild steatosis than AC and MRI-PDFF.
Conclusion: Measurement of ACs in US studies by devices from different vendors compared to other modalities of radiological imaging (MDCT and MRI-PDFF) by special phantoms is an accurate and promising method for noninvasive quantification of hepatic steatosis.

* Corresponding author. Doctor of Medicine, Endocrinology Department, Bogomolets National Medical University, 01601, Pushkinska 22a str., Kyiv, Ukraine.
E-mail address: nazariikobyliak@gmail.com (N. Kobyliak).

https://doi.org/10.1016/j.heliyon.2023.e20642
Received 11 May 2023; Received in revised form 3 October 2023; Accepted 3 October 2023
Available online 4 October 2023

1. Introduction

Nonalcoholic fatty liver disease (NAFLD) is the most common human pandemic, affecting 25–40% of the adult population, as well as adolescents and children [1,2]. Recently 236 panellists from 56 countries (multi-society Delphi consensus), given the etiology and pathogenesis propose to replace NAFLD was metabolic dysfunction-associated steatotic liver disease (MASLD) [3].

Today, it is well known that the basis of pathological synthesis and accumulation of lipids in hepatocytes is the metabolic aggression of carbohydrates. The natural course of MASLD inevitably leads to the development of an inflammatory-necrotic scenario, non-alcoholic steatohepatitis (NASH), with further progression to hepatic fibrosis and cirrhosis [4]. Steatosis is a factor in both hepatic (hepatocellular carcinoma, HCC) [5] and extrahepatic carcinogenesis (in particular, colorectal carcinoma, CRC) [6]. Moreover, MASLD is an inducer of atherogenesis and an independent predictor of cardiovascular and cerebrovascular outcomes [7]. The second important population factor for hepatic steatosis is alcohol-associated fatty liver as part of alcoholic liver disease (ALD) [8].

Clinically, MASLD can be diagnosed after excluding other liver diseases (ALD, drug-induced, chronic viral hepatitis, congenital and autoimmune liver disease) [9]. In addition, MASLD may coexist with other liver diseases. Therefore, a diagnosis of MAFLD is plausibly proven as a diagnosis of exclusion in clinical practice [10].

To date, there are no reliable and specific clinical, anthropometric, and biochemical tests for the early diagnosis of fatty liver with the ability to screen the entire population [11]. Biopsy is not the "gold standard" for the diagnosis of hepatic steatosis due to the heterogeneous distribution of fat in the liver, inaccessibility, invasiveness, and cost [12]. Significant hopes for the effectiveness of steatosis detection are given by radiological methods: a family of ultrasound (US) techniques, multidetector computed tomography (MDCT), and a number of techniques based on magnetic resonance imaging (MRI) [13]. The main innovation in US of fatty liver is the measurement of the attenuation coefficient (AC), which allows the quantification and grading of steatosis [14,15]. An important aspect that determines the diagnostic accuracy of US for steatosis is operator dependence [14,15]. It has even been proposed to determine the amount of liver fat and, accordingly, the degree of hepatic steatosis using several radiological modalities simultaneously - US, CT, MRI [16]. It is generally accepted that magnetic resonance proton density fat fraction (MRI-PDFF) has excellent diagnostic value for the assessment of hepatic fat content and the classification of histologic steatosis in patients with MASLD [17]. With high sensitivity and specificity, MRI-PDFF was used to determine MASLD in both adult and paediatric populations [18,19]. This procedure applies to both simple steatosis and steatohepatitis in the background of MASLD [19,20].

MRI has high reproducibility between different MR platforms and manufacturers in MRI-PDFF technology for liver steatometry [21]. Quantitative determination of steatosis has been successfully achieved for both ALD and MASLD using different MRI technologies compared to liver biopsy data [22]. What seems particularly important for the early diagnosis of MASLD is the ability and sensitivity of MRI-PDFF to find a mild degree of hepatic steatosis [23]. MRI techniques such as MRI-PDFF and MR spectroscopy (MRS) often serve as references for various methods of US steatometry [24–26].

The use of ultrasound steatometry compared to MRI-PDFF and MDCT has significant advantages in screening for hepatic steatosis in order to overcome this pandemic. Ultrasound steatometry has such advantages as easy performance, equipment mobility, low cost, greater availability, and the ability to monitor the dynamics of liver steatosis. In addition, it is also safer compared to MRI (strong magnetic field, which requires strict safety rules, long-term study, risk of claustrophobia) and MDCT (negative effect of ionizing radiation) [13–15].

The aim of the present study was to evaluate the accuracy and reproducibility of real-time US steatometry with AC measurement compared with steatometry using MDCT and MRI-PDFF on a series of phantom simulators with different ratios of fat and water.

2. Materials and methods

2.1. Study design

The study protocol was approved by the Ethics Committee at Bogomolets National Medical University (protocol number: 139/2020). This study was conducted between January 2021 and October 2021. The comparison of instrumental methods for assessing and grading hepatic steatosis using a multimodal phantom simulator of different fat and water ratios was performed. The study involved 3 radiological centers. The Varta Medical Center of Vision Partner LLC had a Toshiba Titan 1.5 (Canon Medical Systems, Japan) magnetic resonance imaging scanner with proton density software module (MRI-PDFF) and a 128-slice Aquilion TSX-101 A multidetector computed tomography scanner (Canon Medical Systems, Japan). The MediScan Group LLC Medical Center had an Aplio i900 US system (Canon MS, Japan, device weight approximately 100 kg) with a PVI-475BX convex probe, 4.0 MHz basic frequency, 1.8–6.4 MHz displayed frequency range, 70° field of view/angle, and 50 mm curvature for steatosis assessment via attenuation imaging (ATI) measurement in dB/cm/MHz. The Institute of Elastography LLC Medical Center had a HandyUSound US system (Smart Medical Products Company, Ukraine, weight 3 kg) with a C106E convex probe, 3.5 MHz basic frequency, 1.5–5.0 MHz displayed frequency range, 70°field of view/angle of, and 60 mm curvature with steatosis assessment by determining the attenuation coefficient measurement (ACM) in dB/cm. ACs were measured five times in each phantom sample, and the mean value was calculated. On the same day, phantom steatometry was determined by MDCT and MRI-PDFF.

2.2. Phantom preparation

Modelling of hepatic steatosis for MRI, CT, and ultrasound has a long history [27]. We created a multimodal steatophantom from a container (box) of nonmagnetic material (plastic, waxed paper). The volume of the box was filled with a mixture of semolina, water,

and a suspension of fat (natural milk and cream) in different proportions. The box has an open top surface for acoustic contact with the ultrasound probe. A 3–4 mm flat sponge (foam rubber) was placed on the bottom of the box as a damper to eliminate ultrasound reverberations. Cooked semolina creates a fine-grained image in B-mode, like the echogram of the liver parenchyma. Seventy-four phantoms were made for research with different concentrations of whole milk and diluted with water: 1%, 2.5%, 3.2% and cream: 5%, 8%, 10%, 12%, 15%, 20%, and 22%. The natural composition of milk has a state of suspension consisting of spherical drops of triglycerides that are protein-stabilized and similar to the 0.2–10 μm fatty vacuoles of hepatocytes [28]. The fat globules selected from milk have size about 1–1.5 μm [29,30]. The attenuation coefficient is a method of ultrasonic steatometry based on determining the reflection, scattering and absorption of ultrasonic waves by fat drops of a certain size and concentration. Varying the concentration of milk with different fat content allows us to accurately model different degrees of steatosis.

It is important that none of the radiologists knew the exact concentration of milk in advance using all methods (ultrasound, MRI, MDCT). Thus, this was a blinded study. The possible variability and uncertainty in the phantom preparation was precisely the imitation of real patients, when the researcher cannot know in advance what degree of hepatic steatosis he will be dealing with.

2.3. US steatometry

In accordance with the requirements of the Canon MS Ultrasound Protocol for Human Steatometry - Attenuation Imaging (ATI), we performed a study of our steathophantoms. The parameters of the Aplio i900 diagnostic ultrasound system (Canon Medicsl Systems, Japan) for steatometry were a weight of approximately 100 kg, a PVI-475BX transducer, a 4.0 MHz basic frequency, a 1.8–6.4 MHz displayed frequency range, a 70° field of view/angle, and a 50 mm curvature. The Acquisition Protocol was as follows: 1. The acoustic window is used with better B-mode images; 2. The probe is applied perpendicular to the top surface of the phantom, and the surface is displayed horizontally on the screen; 3. The image is frozen if it contains an ROI free of artifacts or shadows.

The phantom studies used specific parameters and scan settings optimized for hepatic steatosis assessment for ultrasound systems (Aplio i900 and HandyUSound): i900 (convex probe: i8CX1. Curve 70°, range of frequency - 1,8–6,4 MHz, scaning frequency – 3,0 MHz; range of scanning depth 0–11 cm, size of the region of interest (ROI): depth 1–8 cm, width 5 cm), HandyUsound (convex probe C205E; curve 50°, range of frequency - 1,5-5,0 MHz, scanning frequency – 3,0 MHz, range of scanning depth 0–10 cm; size of the region of interest (ROI): depth 2–9 cm, width 4,5 cm). These settings were consistent for all measurements.

The measurement of ROI is automatically outlined in the yellow box. The system automatically marked the artifact from the surface of the phantom in orange. We placed the ATI ROI just below the orange zone of the artifact. The upper border ROI was placed 1 cm deeper from the surface of the phantom. We avoided dark blue areas. The US system check of the coefficient of determination goodness of fit indicated an R2 > 90% was excellent. The reliability criteria were an $R^2 \geq 0.90$ (displayed on the screen in white below the grayscale image). If the reliability criterion was $R^2 < 0.85$ (displayed in yellow), we restarted the acquisition. We used the median value after 10 acquisitions. For staging liver steatosis, we used the scale created by Jae Seok Bae et al., 2019 (dB/cm/MHz): no steatosis (S0) < 0.63; mild steatosis (S1) < 0.70; moderate steatosis (S2) > 0.70; severe steatosis >0.75 [31].

In accordance with the requirements of the US steatometry protocol by ACM in dB/cm, we performed an investigation on a series of phantom simulators with the HandyUSound ultrasound system (Smart Medical Products, Ukraine). The parameters of the HandyU-Sound diagnostic ultrasound system for steatometry were a weight of 3 kg, a C106E transducer, a basic frequency of 3.5 MHz, a displayed frequency range of 1.5–5.0 MHz, a field of view/angle of 70°, and a curvature of 60 mm.

We placed the ACM ROI just below the zone of the artifact. We estimated it by the uneven part of the profilogram. The upper border ROI was placed 1 cm deeper from the surface of the phantom. The operator always fixed the anterior-posterior size of the ROI at a depth of more than 4 cm in the linear part of the profilogram for correct acoustic measurement of the attenuation coefficient. We used the median value after 5 acquisitions.

To stage ACM steatosis according to ACM (dB/cm), we used the scale by Sasso M. et al., 2010: no steatosis (S0) < 2.22; mild steatosis (S1) > 2.22; moderate steatosis (S2) > 2.33; severe steatosis >2.90 [32].

2.4. Quantification of liver fat content by MDCT

We performed multidetector computed tomography (MDCT) of the steatophantoms with a 128-slice Aquilion TSX-101 A CT (Toshiba Medical Systems Corporation), CLX. The protocol included 120 kV, 100 mA, 50 mAs, a pitch factor of 0.828, a thickness of 0.5, a rotation time of 0.4, a filter - body standard, an FC07 cernel, and an ROI diameter of 10–15 mm.

2.5. Quantification of liver fat content by MRI-PDFF

We performed MRI-PDFF of the steatophantoms with thel same protocol for the human liver. The protocol included a COR WFS – TR of 6.2 ms, a TE of 00 ms, a thickness of 10.0 mm, an FOV of 350 × 350, a 96 × 96 matrix, an AX WFS - TR of 6.2 ms, a TE of 00 ms, a thickness of 10.0 mm, an FOV of 350 × 350, a 96 × 96 matrix, and an ROI diameter of 10–15 mm.

2.6. Statistical analyses

Statistical analysis was performed using standard SPSS version 20.0 software (SPSS, Inc., Chicago, Illinois) and GraphPad Prism, version 6.0 (GraphPad Software, Inc., La Jolla, CA, USA). Quantitative changes are presented as the median and 25th and 75th quartiles. Pearson correlation coefficients (r) were computed to express the degree of linear association between measures. We defined

correlation coefficients as strong if $r > 0.8$ and excellent if $r > 0.9$. Intraobserver agreement for ACM was calculated as the intraclass correlation coefficient (ICC) between the first and second 5 measurements performed by the same operator. Data were considered significant when $p < 0.05$.

3. Results

B-mode images of the phantom were the same for both US systems: Aplio i900 and HandyUSound. The filler of the phantom was similar to the natural liver parenchyma, such as a gray fine-grained field. The damper sponge appeared as a hyperechoic linear reflection at the bottom of the phantom.

Colour mapping of the ATI ROI phantom in US steatometry mode on the Aplio i900 looked identical to a human liver image. In the case of the complete absence of fat in the phantom filler, the ATI was less than <0.60 dB/cm/MHz. If the fat content in the phantom was low, the ATI index was <0.60 dB/cm/MHz. This finding meant, according to the generally accepted scale, that the stage was absence of steatosis (S0). In the event that there was too much fat in the phantom filler compared to the human liver, ATI has a strong orange display and measured well over 0.75 dB/cm/MHz. Intermediate concentrations of phantom fat ranged from 0.60 to 0.75 dB/cm/MHz. These ATI values on the steatosis staging scale were in the S1–S2 range (Fig. 1A–D).

When using the HandyUSound US diagnostic system to visualize the attenuation coefficient measurement (ACM) for real-time liver US steatometry of multimodal phantoms, there were similar patterns as for ATI. In the case of the complete absence of fat in the phantom filler, the ACM was less than 2.22 dB/cm. If the fat content in the phantom was low, the ACM was <2.22 dB/cm. This finding meant, according to Sasso's grading scale, the stage was the absence of steatosis (S0). In the event that there was too much fat in the phantom filler compared to the human liver, the ACM ROI had a strong red color and measured well over 2.90 dB/cm. Intermediate concentrations of fat ranged from 2.22 to 2.90 dB/cm. These ACM values on the grading scale were in the S1–S2 range (Fig. 2A–F).

CT scan images of the phantom series with different fat content in the filler, or even without fat, were similar to the CT scan images of the natural liver parenchyma, like a gray fine-grained field. Measurement of density multimodal simulators/phantoms in Hounsfield units by multidetector computer tomography with an Aquilion TSX-101 A in axial and coronal sections of phantoms with different fat contents are presented in (Fig. 3A–D).

Measurement of the proton density of the fat fraction (PDFF) of multimodal simulators/phantoms using magnetic resonance

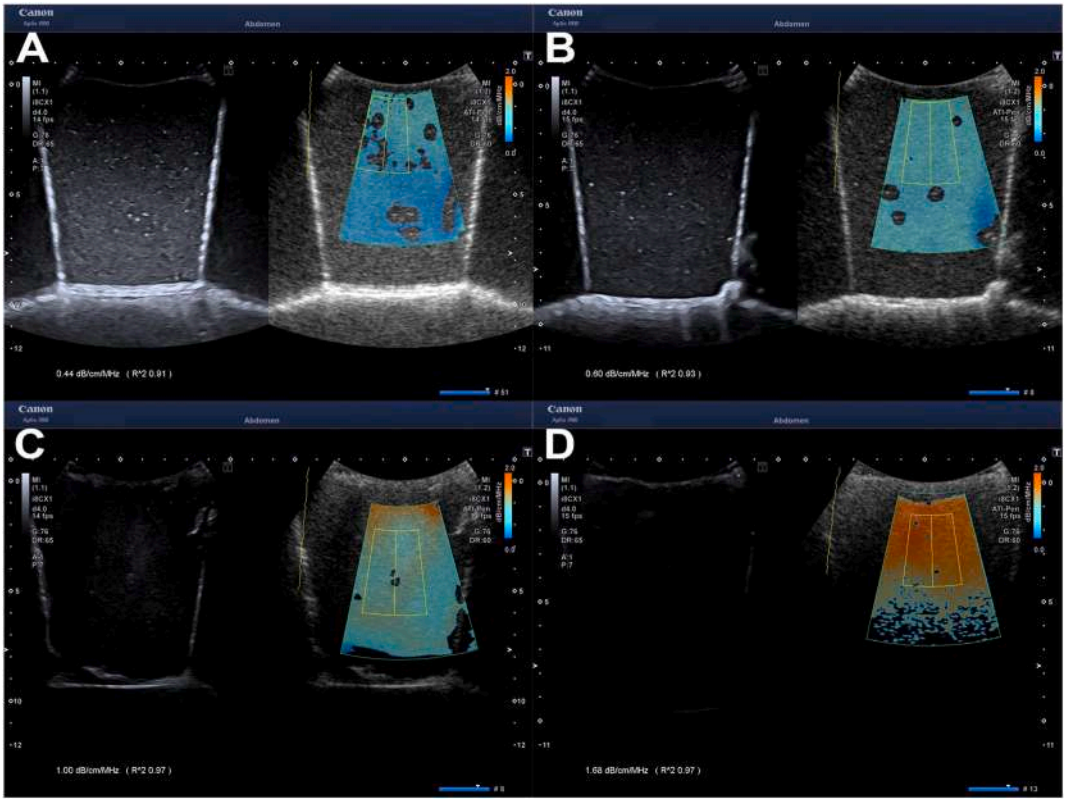

Fig. 1. Measurement Attenuation Imaging (ATI) for real-time ultrasound hepatic steatometry of multimodal simulators/phantoms by the diagnostic ultrasound system Aplio i900 (Canon Medical Systems, Japan). A: fat is completely absent in the phantom filler, no steatosis (S0), ATI = 0,44 (<0,60) dB/cm/MHz; B: no steatosis (S0), ATI = 0,60 dB/cm/MHz; C: severe steatosis, ATI = 1,00 (>0,75) dB/cm/MHz; D: too much fat in the phantom filler than in humans with hepatic steatosis ATI = 1,68 (more than >0,75) dB/cm/MHz.

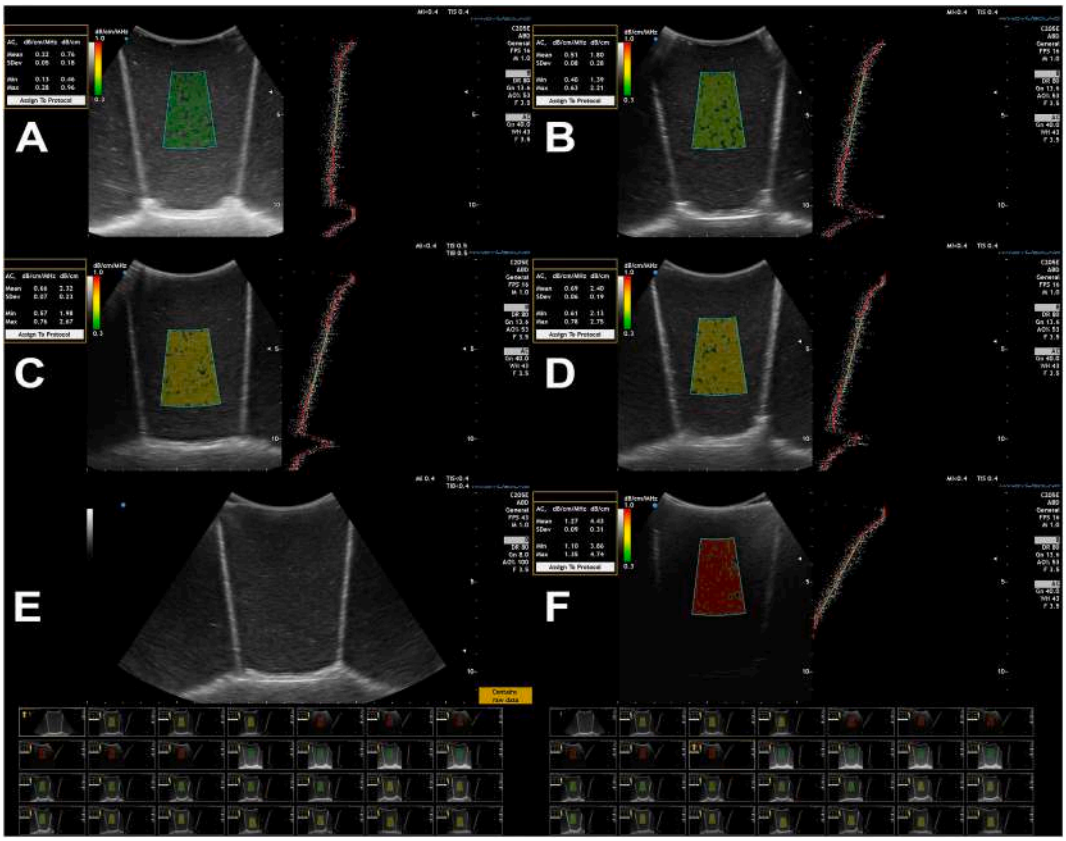

Fig. 2. Attenuation Coefficient Measurement Imaging (ACM) for real-time ultrasound hepatic steatometry of multimodal simulators/phantoms by the diagnostic ultrasound system HandyUSound (Smart Medical Products, Ukraine). **A:** absence fat, ACM = 0,22 dB/cm/MHz or 0,76 dB/cm; **B:** no steatosis (S0), ACM = 0,51 dB/cm/MHz or 1,80 dB/cm; **C:** mild steatosis (S1), ACM = 0,66 dB/cm/MHz or 2,32 dB/cm; **D:** moderate steatosis (S2), ACM = 0,69 dB/cm/MHz or 2,40 dB/cm; **E:** B-mode. Acoustic damper - sponge (3–5 mm thick) on the bottom of the container. **F:** too much fat in the phantom filler than in humans with hepatic steatosis, ACM = 1,27 dB/cm/MHz or 4,43 dB/cm.

imaging with a Toshiba Titan 1.5 (Canon Medical Systems Corporation, Japan) on axial sections of a series of phantoms with different fat contents in the filler and was represented by color mapping on the proton density scale. Blue color represents a filler without fat or with fat below the steatosis cutoff. Yellow on the scale indicates moderate steatosis (S1), orange indicates moderate steatosis (S2), and red indicates severe steatosis (S3). The proton density was measured inside the ROI circle and presented in % (Fig. 4A and B). Overall, the median value [25 and 75 quartiles] of US ACM (dB/cm) and ATI (dB/cm/MHz) and fat percentage by MRI-PDFF (Fat%) and MDCT (Hounsfield Units) were 1.36 [0.80–3.15], 0.57 [0.46–1.01], 29.63 [4.99–93.82], and 42.3 [32.5–51.5], respectively (Fig. 5A–D).

A high, direct correlation was detected between both ACs with Pearson's correlation coefficients of $r = 0.932$ ($p < 0.001$; Fig. 6A). The use of MRI-PDDFF as a reference to ultrasound techniques of the ACs of two manufacturers showed their close correlations with the use of a series of phantoms. However, a more pronounced connection was detected for the ACM ($r = 0.746$, $p > 0.001$; Fig. 6B) than for the ATI ($r = 0.708$, $p > 0.001$; Fig. 6D). The strength of the correlation for both ACs was higher than that for MDCT ($r = -0.623$, $p > 0.001$; Fig. 6F). On the other hand, both US ACs, with a preference for ATI ($r = -0.593$, $p > 0.001$; Fig. 6E), moderately inversely correlated with CT attenuation ($r = -0.581$, $p > 0.001$; Fig. 6C, for ACM). The intraclass correlation coefficient for ACM was 0.944 (95% CI 0.902–0.971, $p < 0.001$).

4. Discussion

Significant hopes for the effectiveness of hepatic steatosis detection are given by radiological methods: a family of US techniques, MDCT, and a number of MRI techniques. The main innovation in abdominal US is the measurement of AC, which allows the quantification and grading of steatosis [13]. The question arises as to what radiological modalities (US, MDCT, MRI) and what technologies are best to use and in which clinical cases: screening, primary and secondary diagnosis, graft evaluation, monitoring/follow up of natural history, and therapeutic and postoperative hepatic steatosis [33]. Development and implementation of US steatometry (traditional B-mode and B-mode dependent – hepato-renal index and US histogram analysis, as well as the latest – AC, backscattering, and speed of sound (SOS) or velocity of US waves through the liver parenchyma) are based on MRI and MDCT methods as references [34].

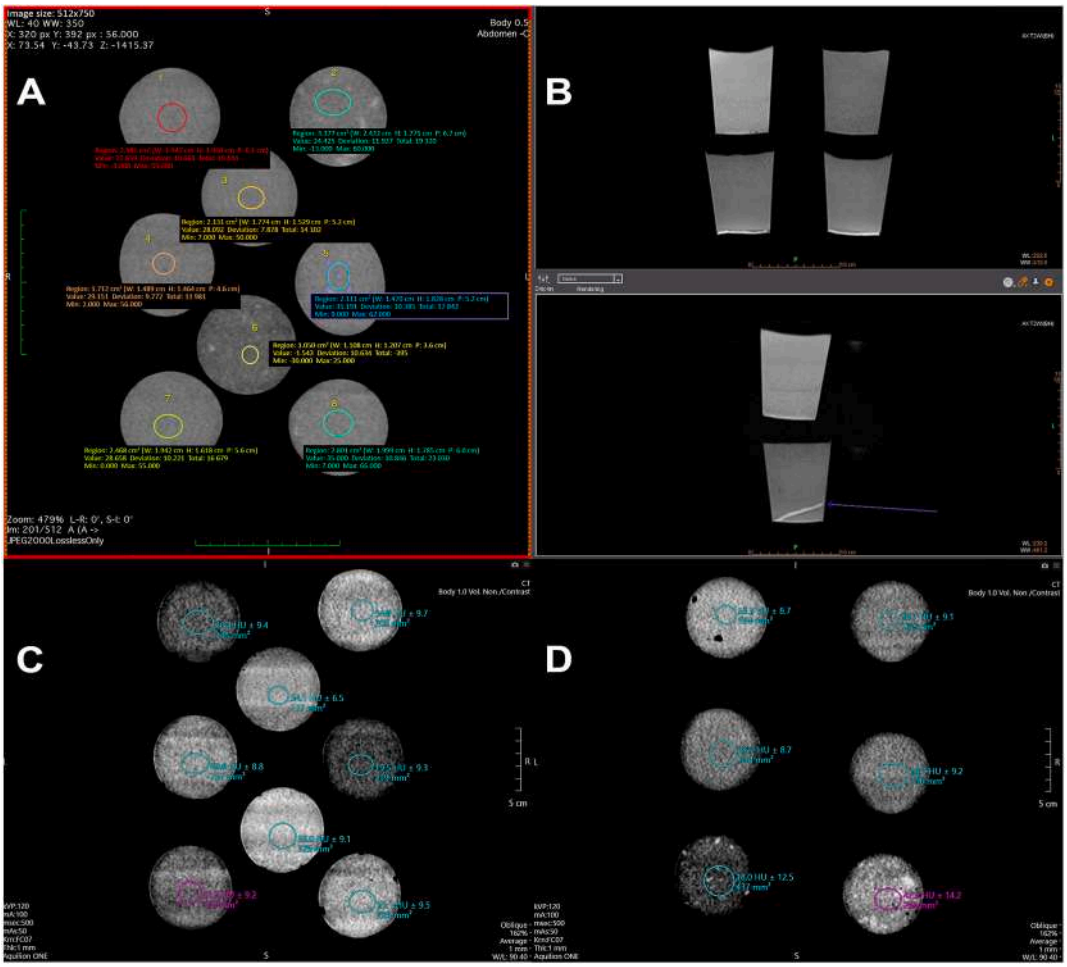

Fig. 3. Measurement of density multimodal simulators/phantoms in HU by multi-detector computer tomography Aquilion TSX-101 A (Toshiba Medical Systems Corporation, Japan). **A, C, D**: axial and sagittal sections of phantom series with different fat content in the filler, or even without fat; **B:** displacement of the acoustic damper (sponge) in one of the phantoms in the direction from the bottom to the filler (arrow). HU - hounsfield units.

Steatotic liver phantoms make it possible to overcome the barrier of newness for novice operators and to master the US steatometry method more easily and quickly. The absence of such traditional difficulties during scanning as interference from ribs and gases (lungs, intestines) allows the operator to focus on the essence of performing the steatometry procedure itself and obtaining stable results.

The results of the current study show that both ACs in phantom studies are more accurate than MDCT for the detection and quantification of hepatic steatosis ($r > 0.7$) when compared with MRI-PDFF as a reference. At one time, the controlled attenuation parameter (CAP™, FibroScan) was the first accurate US diagnosis in the world available to quantify hepatic steatosis, and it became useful equipment for point-of-care US (POCUS) [24,35,36]. Studies that compared CAP and ACs to MRI-PDFF (as the gold standard) showed that ACs are more accurate for quantifying hepatic steatosis [37,38].

The advantage of AC with quantitative assessment of hepatic steatosis is that it is implemented in US systems together with the B-mode anatomical format of assessment of the liver and related organs, 2D share wave elastography (2D SWE) with measurement of liver stiffness for assessment of fibrosis, and Doppler assessment of splanchnic blood flow in portal hypertension. Such technologies in modern US devices allow the implementation of the so-called multiparametric ultrasound (mp-US) approach, which can help reduce the cost of assessing patients with chronic liver disease [13,39,40]. Using AC, modern US devices allow the use of accurate navigation of the ROI to improve the accuracy of steatosis measurement. The criteria for high-quality visualization and navigation of the ROI are color coding, the degree of attenuation, and the attenuation graph of US waves with depth (profilograms). Thus, it is possible to qualitatively visualize areas of interest in the liver parenchyma, avoid artifacts (reverberations, shadows, etc.), and exclude the measurement of undesirable anatomical structures in the ROI. These features of ultrasound devices can contribute to better AC performance compared to CAP and reproducibility of measurements [24]. The creation of a hand-held US device (HHUSD) with AC technology opens the prospect of its widespread use in population studies of MASLD and equipment for POCUS by general practitioners.

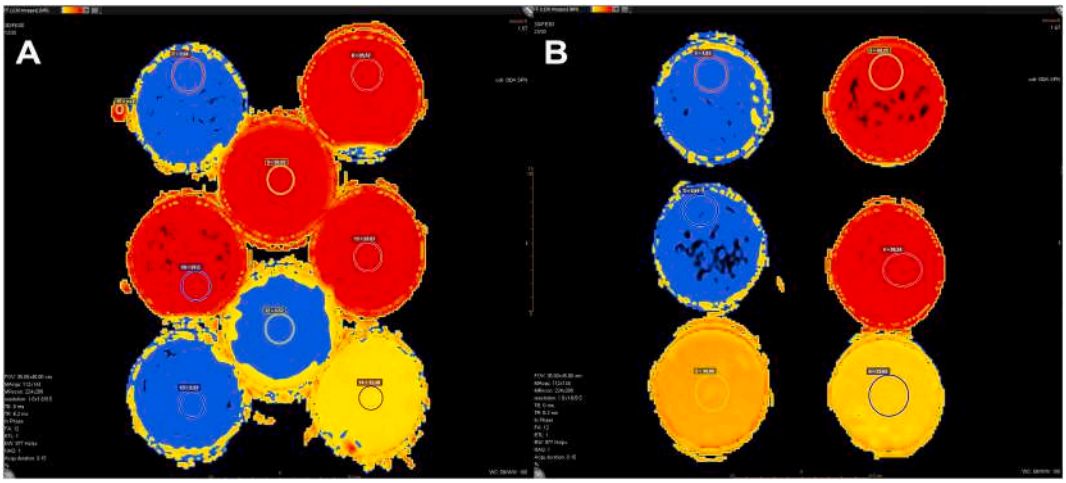

Fig. 4. Measurement of proton density fat fraction (PDFF) of the multimodal simulators/phantoms by magnetic resonance imaging Toshiba Titan 1.5 (Canon Medical Systems Corporation, Japan). **A-B**: axial sections of phantom series with different fat content in the filler: blue – filler without fat or no steatosis; yellow - mild steatosis (S1); orange - moderate steatosis (S2); red - severe steatosis (S3). (For interpretation of the references to color in this figure legend, the reader is referred to the Web version of this article.)

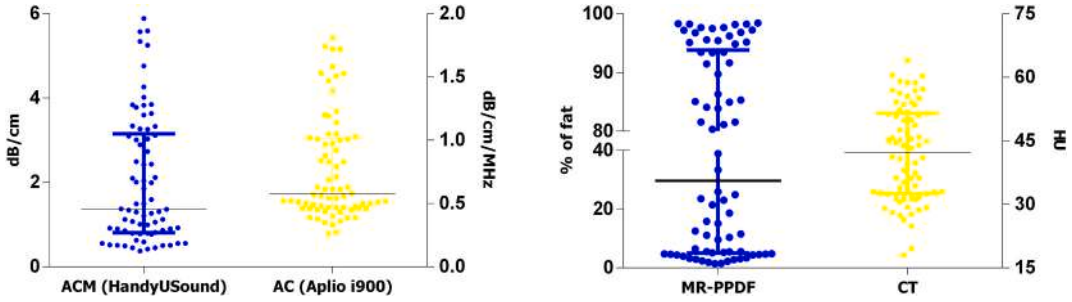

Fig. 5. Plots of phantom measurements by ACs (**A, B**), MRI-PDFF (**C**), and MDCT (**D**). The lines in each diagram represent median value, 25th and 75th quartiles.

Recently, MASLD has become a serious public health problem with a global prevalence of 25–30% for adults and adolescents [41]. The metabolic inability of the liver to control the homeostasis of lipids and coagulation parameters are risk factors for atherosclerosis, cardiovascular disease, and severity of COVID-19 [42–45]. To date, there is no pharmacological drug for targeted therapy of MASLD. The main concept is the timely strength of lifestyle modifications, which has been shown to lead to reverse development and disappearance of steatosis [46]. Thus, for modern medicine, there is a challenge to have methods for early and accurate detection of hepatic steatosis in the general population [47]. AC has a high repeatability of measurements, which is an advantage for further monitoring of the course of MASLD both in natural progression and in response to treatment. Metabolic factors can trigger inflammatory and necrotic scenarios in the liver and progress to NASH [48].

The results of our study and other studies show that ACM is a very valuable and affordable marker of instrumental diagnosis and early detection of hepatic steatosis. For this reason, the exact noninvasive stratification of steatosis is of great interest. MRI-PDFF is a generally accepted reference standard for the assessment of hepatic steatosis. The advantages of using US diagnostics are that it has lower economic costs and greater availability of US equipment. The use of cheap and manual US devices with modern and legible AC modes opens the prospect of their widespread use by general practitioners for screening and dynamic monitoring of hepatic steatosis [49]. Portable US devices with ACM seem to be a very promising tool for the diagnosis of both mild (S1) and moderate (S2) steatosis, which was proven in our study on a series of phantoms and in a pilot study in patients with chronic liver disease compared with the MRI-PDFF reference method.

5. Conclusion

Modeling of hepatic steatosis using a series of phantom simulators allows evidence-based medicine to determine the diagnostic accuracy of the latest US techniques for steatosis. Measurement of ACs in US studies by devices from different vendors compared to other modalities of radiological imaging (MDCT and MRI-PDFF) by special phantoms is an accurate and promising method for noninvasive quantification of hepatic steatosis. The ACM and ATI of both US systems on phantoms correlated well with each other and

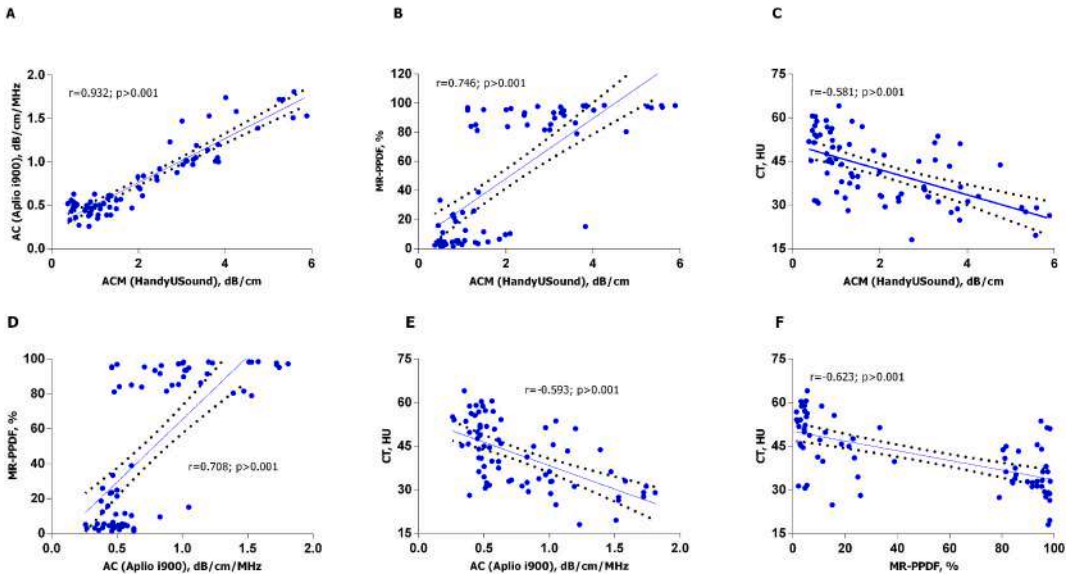

Fig. 6. Pearson correlation analysis between ACs measured by US and radiological imaging in phantom study. **A** – ACM *vs* AC; **B** – ACM *vs* MRI-PDFF; **C** – ACM *vs* MDCT; **D** – AC *vs* MRI-PDFF; **E** – AC *vs* MDCT; **F** - MRI-PDFF *vs* MDCT.

with MRI-PDFF and, thus, can provide good diagnostic value in the assessment of hepatic steatosis. MDCT was less sensitive to mild steatosis than AC and MRI-PDFF.

Funding statement

This research did not receive any specific grant from funding agencies in the public, commercial, or not-for-profit sectors.

Data availability statement

Data will be made available on request.

CRediT authorship contribution statement

Nazarii Kobyliak: Conceptualization, Formal analysis, Investigation, Writing – original draft, Writing – review & editing. **Oleh Dynnyk:** Conceptualization, Investigation, Methodology, Project administration, Supervision, Writing – original draft, Writing – review & editing. **Maryana Savytska:** Resources, Software, Writing – review & editing. **Oleksandr Solodovnyk:** Investigation, Software, Visualization, Writing – review & editing. **Oleksandr Zakomornyi:** Formal analysis, Methodology, Software, Validation, Writing – review & editing. **Oleksii Omelchenko:** Resources, Software, Supervision, Writing – review & editing. **Anton Kushnir:** Formal analysis, Investigation, Software, Visualization, Writing – review & editing. **Roman Titorenko:** Formal analysis, Software, Visualization, Writing – review & editing.

Declaration of competing interest

The authors declare that they have no known competing financial interests or personal relationships that could have appeared to influence the work reported in this paper.

Acknowledgments

None to declare.

Abbreviations

AC	attenuation coefficient
ACM	attenuation coefficient measurement
ALD	alcoholic liver disease
ATI	attenuation imaging

CAP controlled attenuation parameter
CRC colorectal carcinoma
HHUSD, hand held US device
HCC hepatocellular carcinoma
MRI magnetic resonance imaging
MRI-PDFF magnetic resonance proton density fat fraction
MRS magnetic resonance spectroscopy
MDCT multidetector computed tomography
MASLD metabolic dysfunction-associated steatotic liver disease
NASH non-alcoholic steatohepatitis
POCUS, point-of-care US
ROI region of interest
US, ultrasound

References

[1] T.G. Cotter, M. Rinella, Nonalcoholic fatty liver disease 2020: the state of the disease, Gastroenterology 158 (2020) 1851–1864, https://doi.org/10.1053/j.gastro.2020.01.052.

[2] Z. Younossi, F. Tacke, M. Arrese, B. Chander Sharma, I. Mostafa, E. Bugianesi, V. Wai-Sun Wong, Y. Yilmaz, J. George, J. Fan, M.B. Vos, Global perspectives on nonalcoholic fatty liver disease and nonalcoholic steatohepatitis, Hepatology 69 (2019) 2672–2682, https://doi.org/10.1002/hep.30251.

[3] M.E. Rinella, J.V. Lazarus, V. Ratziu, S.M. Francque, A.J. Sanyal, F. Kanwal, D. Romero, M.F. Abdelmalek, Q.M. Anstee, J.P. Arab, M. Arrese, R. Bataller, U. Beuers, J. Boursier, E. Bugianesi, C. Byrne, G.E. Castro Narro, A. Chowdhury, H. Cortez-Pinto, D. Cryer, K. Cusi, M. El-Kassas, S. Klein, W. Eskridge, J. Fan, S. Gawrieh, C.D. Guy, S.A. Harrison, S.U. Kim, B. Koot, M. Korenjak, K. Kowdley, F. Lacaille, R. Loomba, R. Mitchell-Thain, T.R. Morgan, E. Powell, M. Roden, M. Romero-Gómez, M. Silva, S.P. Singh, S.C. Sookoian, C.W. Spearman, D. Tiniakos, L. Valenti, M.B. Vos, V. Wai-Sun Wong, S. Xanthakos, Y. Yilmaz, Z. Younossi, A. Hobbs, M. Villota-Rivas, P.N. Newsome, V. Ajmeral, W. Alazawi, M. Alkhatry, N. Alkhouri, A. Allen, M. Allison, K. Alswat, M.R. Alvares-da-Silva, M. Alves-Bezerra, M.J. Armstrong, D. Arufe, P. Aschner, G. Baffy, M. Bansal, P. Bedossa, R. Belfort, T. Berg, A. Berzigotti, M. Betel, C. Bianco, C. Brass, C. L. Brosgart, E.M. Brunt, M. Buti, S. Caldwell, R. Carr, T. Casanovas, L. Castera, C. Caussy, E. Cerda, N. Chalasani, W.K. Chan, P. Charatcharoenwitthaya, M. Charlton, A. Cheung, D. Chiodi, R. Chung, D. Cohen, K. Corey, H.P. Cotrim, J. Crespo, A. Dassanayake, N. Davidson, R. De Knegt, V. De Ledinghen, M. Demir, S. Diaz, A.M. Diehl, B. Dimmig, M. Dirchwolf, A. Duseja, K. Dvorak, M. Ekstedt, R. El Wakil, M.L. Ferraz, S. Friedman, M. Fuchs, A. Gastaldelli, A. Geerts, A. Geier, M. Girala, G. Goh, N. Goossens, I. Graupera, H. Hagström, Z. Henry, B. Hunyady, A. Hutchison, S. Isaacs, F. Jornayvaz, C. Kemp, D. Kile, W. Kim, D. Kleiner, R. Kohli, M. Kugelmas, J. Lavine, M. Lazo, N. Leite, A. Lozano, P. Luukkonen, P. Macedo, D. Mansour, C. Mantzoros, G. Marchesini, S. Marciano, K. Martinez, L.V. Mateva, J.M. Mato, A. McCary, L. Miele, I. Mikolasevic, V. Miller, R. Moreno, C. Moylan, A. Nakajima, J.C. Nault, S. Norris, M. Noureddin, C. P. Oliveira, A. Ong, M. Padilla, R. Pais, A. Panduro, M.K. Panigrahi, G. Papatheodoridis, S. Pelusi, M. Pérez, J.P. Escobar, G. Perseghin, M. Pessoa, S. Petta, M. Pinzani, M.P. Lupsor, A. Rabiee, S. Romeo, Y. Rotman, I. Rowe, R. Salupere, S. Satapathy, J.M. Schattenberg, W. Schaufert, B. Schnabl, L. Seim, L. Serfaty, D. Shapiro, A.K. Singal, L. Skladany, N. Stefan, J. Stine, S. Sundaram, G. Svegliati-Baroni, G. Szabo, F. Tacke, T. Tanwandee, G. Targher, N. Terrault, B. Tetri, M. Thiele, B. Tisthammer, A.T. Delgadillo, M. Trauner, E. Tsochatzis, L. Van Kleef, S. Van Mil, L. VanWagner, J.A. Velarde Ruiz Velasco, M. Vesterhus, E. Vilar-Gomez, K. Watt, J. Wattacheril, F. Wilkins, J. Willemse, A. Zekry, S. Zelber-Sagi, A multi-society Delphi consensus statement on new fatty liver disease nomenclature, J. Hepatol. (2023), https://doi.org/10.1016/J.JHEP.2023.06.003.

[4] G. Mykhalchyshyn, N. Kobyliak, P. Bodnar, Diagnostic accuracy of acyl-ghrelin and it association with non-alcoholic fatty liver disease in type 2 diabetic patients, J. Diabetes Metab. Disord. 14 (2015), https://doi.org/10.1186/s40200-015-0170-1.

[5] D.Q. Huang, H.B. El-Serag, R. Loomba, Global epidemiology of NAFLD-related HCC: trends, predictions, risk factors and prevention, Nat. Rev. Gastroenterol. Hepatol. 18 (2021) 223–238, https://doi.org/10.1038/S41575-020-00381-6.

[6] M. Eslami, S. Sadrifar, M. Karbalaei, M. Keikha, N.M. Kobyliak, B. Yousefi, Importance of the microbiota inhibitory mechanism on the warburg effect in colorectal cancer cells, J. Gastrointest. Cancer 51 (2020) 738–747, https://doi.org/10.1007/s12029-019-00329-3.

[7] D. Stols-Gonçalves, G.K. Hovingh, M. Nieuwdorp, A.G. Holleboom, NAFLD and atherosclerosis: two sides of the same dysmetabolic coin? Trends Endocrinol. Metabol.: TEM (Trends Endocrinol. Metab.) 30 (2019) 891–902, https://doi.org/10.1016/J.TEM.2019.08.008.

[8] E. Ceni, T. Mello, A. Galli, Pathogenesis of alcoholic liver disease: role of oxidative metabolism, World J. Gastroenterol. 20 (2014) 17756–17772, https://doi.org/10.3748/WJG.V20.I47.17756.

[9] Y. Sumida, M. Yoneda, K. Tokushige, M. Kawanaka, H. Fujii, M. Yoneda, K. Imajo, H. Takahashi, Y. Eguchi, M. Ono, Y. Nozaki, H. Hyogo, M. Koseki, Y. Yoshida, T. Kawaguchi, Y. Kamada, T. Okanoue, A. Nakajima, FIB-4 First in the Diagnostic Algorithm of Metabolic-Dysfunction-Associated Fatty Liver Disease in the Era of the Global Metabodemic, vol. 11, 2021, pp. 1–20, https://doi.org/10.3390/LIFE11020143. Life (Basel, Switzerland).

[10] M. Eslam, P.N. Newsome, S.K. Sarin, Q.M. Anstee, G. Targher, M. Romero-Gomez, S. Zelber-Sagi, V. Wai-Sun Wong, J.F. Dufour, J.M. Schattenberg, T. Kawaguchi, M. Arrese, L. Valenti, G. Shiha, C. Tiribelli, H. Yki-Järvinen, J.G. Fan, H. Grønbæk, Y. Yilmaz, H. Cortez-Pinto, C.P. Oliveira, P. Bedossa, L. A. Adams, M.H. Zheng, Y. Fouad, W.K. Chan, N. Mendez-Sanchez, S.H. Ahn, L. Castera, E. Bugianesi, V. Ratziu, J. George, A new definition for metabolic dysfunction-associated fatty liver disease: an international expert consensus statement, J. Hepatol. 73 (2020) 202–209, https://doi.org/10.1016/J.JHEP.2020.03.039.

[11] C. Stern, L. Castera, Non-invasive diagnosis of hepatic steatosis, Hepatology International 11 (2017) 70–78, https://doi.org/10.1007/S12072-016-9772-Z.

[12] N. Kobyliak, O. Dynnyk, L. Abenavoli, The role of liver biopsy to assess alcoholic liver disease, Rev. Recent Clin. Trials 11 (2016), https://doi.org/10.2174/1574887111666160724184103.

[13] G. Ferraioli, A. Berzigotti, R.G. Barr, B.I. Choi, X.W. Cui, Y. Dong, O.H. Gilja, J.Y. Lee, D.H. Lee, F. Moriyasu, F. Piscaglia, K. Sugimoto, G.L.H. Wong, V.W. S. Wong, C.F. Dietrich, Quantification of liver fat content with ultrasound: a WFUMB position paper, Ultrasound Med. Biol. 47 (2021) 2803–2820, https://doi.org/10.1016/J.ULTRASMEDBIO.2021.06.002.

[14] S.R. Mehta, E.L. Thomas, J.D. Bell, D.G. Johnston, S.D. Taylor-Robinson, Non-invasive means of measuring hepatic fat content, World J. Gastroenterol. 14 (2008) 3476–3483, https://doi.org/10.3748/WJG.14.3476.

[15] D.H. Lee, Imaging evaluation of non-alcoholic fatty liver disease: focused on quantification, Clin. Mol. Hepatol. 23 (2017) 290–301, https://doi.org/10.3350/CMH.2017.0042.

[16] Y. Zhang, K.J. Fowler, G. Hamilton, J.Y. Cui, E.Z. Sy, M. Balanay, J.C. Hooker, N. Szeverenyi, C.B. Sirlin, Liver fat imaging-a clinical overview of ultrasound, CT, and MR imaging, Br. J. Radiol. 91 (2018), 20170959, https://doi.org/10.1259/BJR.20170959.

[17] J. Gu, S. Liu, S. Du, Q. Zhang, J. Xiao, Q. Dong, Y. Xin, Diagnostic value of MRI-PDFF for hepatic steatosis in patients with non-alcoholic fatty liver disease: a meta-analysis, Eur. Radiol. 29 (2019) 3564–3573, https://doi.org/10.1007/S00330-019-06072-4.

[18] H.I. Awai, K.P. Newton, C.B. Sirlin, C. Behling, J.B. Schwimmer, Evidence and recommendations for imaging liver fat in children, based on systematic review, Clin. Gastroenterol. Hepatol. : The Official Clinical Practice Journal of the American Gastroenterological Association. 12 (2014) 765–773, https://doi.org/10.1016/J.CGH.2013.09.050.

[19] M.S. Middleton, M.L. Van Natta, E.R. Heba, A. Alazraki, A.T. Trout, P. Masand, E.M. Brunt, D.E. Kleiner, E. Doo, J. Tonascia, J.E. Lavine, W. Shen, G. Hamilton, J.B. Schwimmer, C.B. Sirlin, Diagnostic accuracy of magnetic resonance imaging hepatic proton density fat fraction in pediatric nonalcoholic fatty liver disease, Hepatology (Baltimore, Md 67 (2018) 858–872, https://doi.org/10.1002/HEP.29596.

[20] B. Wildman-Tobriner, M.M. Middleton, C.A. Moylan, S. Rossi, O. Flores, Z.A. Chang, M.F. Abdelmalek, C.B. Sirlin, M.R. Bashir, Association between magnetic resonance imaging-proton density fat fraction and liver histology features in patients with nonalcoholic fatty liver disease or nonalcoholic steatohepatitis, Gastroenterology 155 (2018) 1428–1435.e2, https://doi.org/10.1053/J.GASTRO.2018.07.018.

[21] G.H. Kang, I. Cruite, M. Shiehmorteza, T. Wolfson, A.C. Gamst, G. Hamilton, M. Bydder, M.S. Middleton, C.B. Sirlin, Reproducibility of MRI-determined proton density fat fraction across two different MR scanner platforms, J. Magn. Reson. Imag. : JMRI 34 (2011) 928–934, https://doi.org/10.1002/JMRI.22701.

[22] C. Boudinaud, A. Abergel, J. Joubert-Zakeyh, M. Fontarensky, B. Pereira, B. Chauveau, J.M. Garcier, P. Chabrot, L. Boyer, B. Magnin, Quantification of steatosis in alcoholic and nonalcoholic fatty liver disease: evaluation of four MR techniques versus biopsy, Eur. J. Radiol. 118 (2019) 169–174, https://doi.org/10.1016/J.EJRAD.2019.07.025.

[23] C.C. Park, C. Hooker, J.C. Hooker, E. Bass, W. Haufe, A. Schlein, Y. Covarrubias, E. Heba, M. Bydder, T. Wolfson, A. Gamst, R. Loomba, J. Schwimmer, D. Hernando, S.B. Reeder, M. Middleton, C.B. Sirlin, G. Hamilton, Assessment of a high-SNR chemical-shift-encoded MRI with complex reconstruction for proton density fat fraction (PDFF) estimation overall and in the low-fat range, J. Magn. Reson. Imag. : JMRI 49 (2019) 229–238, https://doi.org/10.1002/JMRI.26168.

[24] G. Ferraioli, L. Maiocchi, M.V. Raciti, C. Tinelli, A. de Silvestri, M. Nichetti, P. de Cata, M. Rondanelli, L. Chiovato, F. Calliada, C. Filice, Detection of liver steatosis with a novel ultrasound-based technique: a pilot study using MRI-derived proton density fat fraction as the gold standard, Clin. Transl. Gastroenterol. 10 (2019), e00081, https://doi.org/10.14309/CTG.0000000000000081.

[25] C. Caussy, M.H. Alquiraish, P. Nguyen, C. Hernandez, S. Cepin, L.E. Fortney, V. Ajmera, R. Bettencourt, S. Collier, J. Hooker, E. Sy, E. Rizo, L. Richards, C. B. Sirlin, R. Loomba, Optimal threshold of controlled attenuation parameter with MRI-PDFF as the gold standard for the detection of hepatic steatosis, Hepatology (Baltimore, Md 67 (2018) 1348–1359, https://doi.org/10.1002/HEP.29639.

[26] J.S. Paige, G.S. Bernstein, E. Heba, E.A.C. Costa, M. Fereirra, T. Wolfson, A.C. Gamst, M.A. Valasek, G.Y. Lin, A. Han, J.W. Erdman, W.D. O'Brien, M.P. Andre, R. Loomba, C.B. Sirlin, A pilot comparative study of quantitative ultrasound, conventional ultrasound, and MRI for predicting histology-determined steatosis grade in adult nonalcoholic fatty liver disease, AJR. American Journal of Roentgenology. 208 (2017) W168, https://doi.org/10.2214/AJR.16.16726. –W177.

[27] H.H. Hu, T. Yokoo, M.R. Bashir, C.B. Sirlin, D. Hernando, D. Malyarenko, T.L. Chenevert, M.A. Smith, S.D. Serai, M.S. Middleton, W.C. Henderson, G. Hamilton, J. Shaffer, Y. Shu, J.A. Tkach, A.T. Trout, N. Obuchowski, J.H. Brittain, E.F. Jackson, S.B. Reeder, Linearity and bias of proton density fat fraction as a quantitative imaging biomarker: a multicenter, Multiplatform, Multivendor Phantom Study, Radiology 298 (2021) 640–651, https://doi.org/10.1148/RADIOL.2021202912.

[28] M.B. Schott, S.G. Weller, R.J. Schulze, E.W. Krueger, K. Drizyte-Miller, C.A. Casey, M.A. McNiven, Lipid droplet size directs lipolysis and lipophagy catabolism in hepatocytes, J. Cell Biol. 218 (2019) 3320–3335, https://doi.org/10.1083/JCB.201803153.

[29] C. Lopez, V. Briard-Bion, O. Ménard, E. Beaucher, F. Rousseau, J. Fauquant, N. Leconte, B. Robert, Fat globules selected from whole milk according to their size: different compositions and structure of the biomembrane, revealing sphingomyelin-rich domains, Food Chem. 125 (2011) 355–368, https://doi.org/10.1016/J.FOODCHEM.2010.09.005.

[30] P. Sharma, I. Oey, D.W. Everett, Interfacial properties and transmission electron microscopy revealing damage to the milk fat globule system after pulsed electric field treatment, Food Hydrocolloids 47 (2015) 99–107, https://doi.org/10.1016/J.FOODHYD.2015.01.023.

[31] J.S. Bae, D.H. Lee, J.Y. Lee, H. Kim, S.J. Yu, J.H. Lee, E.J. Cho, Y. Bin Lee, J.K. Han, B.I. Choi, Assessment of hepatic steatosis by using attenuation imaging: a quantitative, easy-to-perform ultrasound technique, Eur. Radiol. 29 (2019) 6499–6507, https://doi.org/10.1007/S00330-019-06272-Y.

[32] M. Sasso, M. Beaugrand, V. de Ledinghen, C. Douvin, P. Marcellin, R. Poupon, L. Sandrin, V. Miette, Controlled attenuation parameter (CAP): a novel VCTE™ guided ultrasonic attenuation measurement for the evaluation of hepatic steatosis: preliminary study and validation in a cohort of patients with chronic liver disease from various causes, Ultrasound Med. Biol. 36 (2010) 1825–1835, https://doi.org/10.1016/J.ULTRASMEDBIO.2010.07.005.

[33] A. Qayyum, D.M. Chen, R.S. Breiman, A.C. Westphalen, B.M. Yeh, K.D. Jones, Y. Lu, F.V. Coakley, P.W. Callen, Evaluation of diffuse liver steatosis by ultrasound, computed tomography, and magnetic resonance imaging: which modality is best? Clin. Imag. 33 (2009) 110–115, https://doi.org/10.1016/J.CLINIMAG.2008.06.036.

[34] K. Sugimoto, Development of US- and CT/MRI-based quantification of liver steatosis, J. Med. Ultrason. 48 (2021) (2001) 463, https://doi.org/10.1007/S10396-021-01137-8.

[35] T. Karlas, D. Petroff, M. Sasso, J.G. Fan, Y.Q. Mi, V. de Lédinghen, M. Kumar, M. Lupsor-Platon, K.H. Han, A.C. Cardoso, G. Ferraioli, W.K. Chan, V.W.S. Wong, R.P. Myers, K. Chayama, M. Friedrich-Rust, M. Beaugrand, F. Shen, J.B. Hiriart, S.K. Sarin, R. Badea, K.S. Jung, P. Marcellin, C. Filice, S. Mahadeva, G.L. H. Wong, P. Crotty, K. Masaki, J. Bojunga, P. Bedossa, V. Keim, J. Wiegand, Individual patient data meta-analysis of controlled attenuation parameter (CAP) technology for assessing steatosis, J. Hepatol. 66 (2017) 1022–1030, https://doi.org/10.1016/J.JHEP.2016.12.022.

[36] G. Ferraioli, V.W.S. Wong, L. Castera, A. Berzigotti, I. Sporea, C.F. Dietrich, B.I. Choi, S.R. Wilson, M. Kudo, R.G. Barr, Liver ultrasound elastography: an update to the world federation for ultrasound in medicine and biology guidelines and recommendations, Ultrasound Med. Biol. 44 (2018) 2419–2440, https://doi.org/10.1016/J.ULTRASMEDBIO.2018.07.008.

[37] J.H. Runge, L.P. Smits, J. Verheij, A. Depla, S.D. Kuiken, B.C. Baak, A.J. Nederveen, U. Beuers, J. Stoker, MR spectroscopy-derived proton density fat fraction is superior to controlled attenuation parameter for detecting and grading hepatic steatosis, Radiology 286 (2018) 547–556, https://doi.org/10.1148/RADIOL.2017162931.

[38] C.C. Park, P. Nguyen, C. Hernandez, R. Bettencourt, K. Ramirez, L. Fortney, J. Hooker, E. Sy, M.T. Savides, M.H. Alquiraish, M.A. Valasek, E. Rizo, L. Richards, D. Brenner, C.B. Sirlin, R. Loomba, Magnetic resonance elastography vs transient elastography in detection of fibrosis and noninvasive measurement of steatosis in patients with biopsy-proven nonalcoholic fatty liver disease, Gastroenterology 152 (2017) 598–607.e2, https://doi.org/10.1053/J.GASTRO.2016.10.026.

[39] O. Dynnyk, A. Fedusenko, N. Kobyliak, Multiparametric Ultrasound (Mp-US) in the Chronic Diffuse Liver Disease Diagnosis, 2017, https://doi.org/10.1594/ECR2017/C-2865.

[40] O. Dynnyk, N. Marunchyn, Diagnostic Value of Mp-US of the Non-alcoholic Fatty Liver Disease in the Patients with Type 2 Diabetes Mellitus, 2019, https://doi.org/10.26044/ECR2019/C-0736.

[41] Z.M. Younossi, D. Blissett, R. Blissett, L. Henry, M. Stepanova, Y. Younossi, A. Racila, S. Hunt, R. Beckerman, The economic and clinical burden of nonalcoholic fatty liver disease in the United States and Europe, Hepatology (Baltimore, Md 64 (2016) 1577–1586, https://doi.org/10.1002/HEP.28785.

[42] J.H. Kang, K.I. Cho, S.M. Kim, J.Y. Lee, J.J. Kim, J.J. Goo, K.N. Kim, J.H. Jhi, D.J. Kim, H.G. Lee, T.I. Kim, Relationship between nonalcoholic fatty liver disease and carotid artery atherosclerosis beyond metabolic disorders in non-diabetic patients, Journal of Cardiovascular Ultrasound 20 (2012) 126–133, https://doi.org/10.4250/JCU.2012.20.3.126.

[43] Y.J. Zhou, K.I. Zheng, X.B. Wang, Q.F. Sun, K.H. Pan, T.Y. Wang, H.L. Ma, Y.P. Chen, J. George, M.H. Zheng, Metabolic-associated fatty liver disease is associated with severity of COVID-19, Liver International, Official Journal of the International Association for the Study of the Liver 40 (2020) 2160–2163, https://doi.org/10.1111/LIV.14575.

[44] A. Ali, M. Hasan, S. Hamed, A. Elhamy, Hepatic steatosis: a risk factor for increased COVID-19 prevalence and severity-a computed tomography study, Egyptian Liver Journal 11 (2021) 61, https://doi.org/10.1186/S43066-021-00131-6.

[45] I. Gasparova, P. Kubatka, R. Opatrilova, M. Caprnda, S. Filipova, L. Rodrigo, L. Malan, I. Mozos, M. Rabajdova, V. Nosal, N. Kobyliak, V. Valentova, D. Petrovic, M. Adamek, P. Kruzliak, Perspectives and challenges of antioxidant therapy for atrial fibrillation, Naunyn-Schmiedeberg's Arch. Pharmacol. 390 (2017) 1–14, https://doi.org/10.1007/s00210-016-1320-9.

[46] G. Marchesini, C.P. Day, J.F. Dufour, A. Canbay, V. Nobili, V. Ratziu, H. Tilg, M. Roden, A. Gastaldelli, H. Yki-Jarvinen, F. Schick, R. Vettor, G. Fruhbeck, L. Mathus-Vliegen, EASL-EASD-EASO Clinical Practice Guidelines for the management of non-alcoholic fatty liver disease, J. Hepatol. 64 (2016) 1388–1402, https://doi.org/10.1016/j.jhep.2015.11.004.

[47] E. Blond, E. Disse, C. Cuerq, J. Drai, P.J. Valette, M. Laville, C. Thivolet, C. Simon, C. Caussy, EASL–EASD–EASO clinical practice guidelines for the management of non-alcoholic fatty liver disease in severely obese people: do they lead to over-referral? Diabetologia 60 (2017) 1218–1222, https://doi.org/10.1007/s00125-017-4264-9.

[48] A. Arulanandan, B. Ang, R. Bettencourt, J. Hooker, C. Behling, G.Y. Lin, M.A. Valasek, J.H. Ix, B. Schnabl, C.B. Sirlin, R. Loomba, Association between quantity of liver fat and cardiovascular risk in patients with nonalcoholic fatty liver disease independent of nonalcoholic steatohepatitis, Clin. Gastroenterol. Hepatol. : The Official Clinical Practice Journal of the American Gastroenterological Association. 13 (2015) 1513–1520.e1, https://doi.org/10.1016/J.CGH.2015.01.027.

[49] I. Sporea, R. Mare, A. Popescu, S. Nistorescu, V. Baldea, R. Sirli, A. Braha, A. Sima, R. Timar, R. Lupusoru, Screening for liver fibrosis and steatosis in a large cohort of patients with type 2 diabetes using vibration controlled transient elastography and controlled attenuation parameter in a single-center real-life experience, J. Clin. Med. 9 (2020), https://doi.org/10.3390/JCM9041032.